Received: 11 December 2020 | Revised: 25 July 2021 | Accepted: 15 September 2021

DOI: 10.1002/navi.454

ORIGINAL ARTICLE

WILEY ION

Study of structures of the sporadic E layer by using dense GNSS network observations

Susumu Saito[1] | **Keisuke Hosokawa**[2] | **Jun Sakai**[2] | **Ichiro Tomizawa**[2]

[1] Electronic Navigation Research Institute, National Institute of Maritime, Port and Aviation Technology, Japan

[2] University of Electro-Communications, Japan

Correspondence
Susumu Saito, Electronic Navigation Research Institute, National Institute of Maritime, Port and Aviation Technology, 7-42-23 Jindaij-Higashi, Chofu, Tokyo 182-0012, Japan.
Email: susaito@mpat.go.jp

Funding information
Japan Society for the Promotion of Science, Grant/Award Number: 18H04437; Murata Science Foundation

Abstract

The sporadic E (Es) layer has been known to introduce long-range propagation of aeronautical very high frequency (VHF) navigation beyond the radio horizon and cause potential interference on the navigation system. This study utilizes a rate of total electron content (TEC) index (ROTI) map with dense Global Navigation Satellite System (GNSS) observations for effective Es layer detection. The daytime Es layer shows a well-defined frontal structure when ROTI values are mapped at the typical Es layer height (100 km). A methodology of detecting and characterizing the Es layer frontal structure without manual operation is developed by utilizing the Hough transform. The front direction and drift velocity are successfully derived. Sub-structures in the Es layer front are revealed by analysis using the characteristics of the frontal structure and TEC variation. The developed method is suitable for an automated real-time Es-layer monitoring system in a wide area.

KEYWORDS

GNSS, ionosphere, sporadic E layer, total electron content

1 | INTRODUCTION

The sporadic E (Es) layer is an ionospheric layer with a high electron density and thin altitudinal thickness appearing at altitudes around 100 km. The density is sometimes so high that even very high frequency (VHF) radio waves from the ground can be reflected and propagate beyond the radio horizon. It has been shown that aeronautical VHF navigation signals in the 108–118 MHz band can propagate beyond the radio horizon to cause potential interference (Sakai et al., 2019).

It has been known that the vertical shear of the neutral wind accumulates metallic ions to generate the Es layer (Whitehead, 1970). It is also known that it often appears in local summer especially in mid-latitude regions (Taguchi & Shibata, 1961). The occurrence of the Es layer is mainly controlled by the shear of the neutral wind [e.g., Shinagawa et al. (2017)]. However, as it appears *sporadically*, prediction of its occurrence has not been realized yet. The peak density of the Es layer is variable from time to time, which adds more difficulty in predicting the Es layer occurrence.

To understand how the Es layer maximum density changes, it is important to understand the development of the structures of the Es layer. However, there are a limited number of studies that show the detailed structures of the Es layer (Maruyama, 1991; Miller & Smith, 1975, 1978; Saito et al., 2006). The study of the Es layer structure in

daytime is difficult because the radar imaging of backscatter from ionospheric irregularities associated with the Es layer cannot be used in daytime when small-scale irregularities are inhibited due to high electric conductivity of the ionosphere (Saito et al., 2006).

Recently, signatures of the Es layer have been identified from Global Navigation Satellite System (GNSS) data analysis. Maeda and Heki (2014) reported the two-dimensional structure of the Es layer by analyzing the perturbation of the ionospheric total electron contents (TECs) observed by GNSS receiving stations, though the perturbation amplitude was small.

Careful manual analysis was needed to detect the Es layer signature. Muafiry et al. (2018) investigated the Es layer signature with a tomographic inversion technique. However, it was difficult to clearly resolve the Es layer structure due to insufficient temporal resolution (TECs sampled every 30 seconds) and spatial resolution.

To observe ionospheric irregularities, the Rate-of-TEC Index (ROTI), which is the standard deviation of the rate of TEC in a certain time interval (Pi et al., 1997), are often used. It is an index easily obtained from observations of normal GNSS receivers without specialized scintillation receivers. Recently, ROTI values have been used to obtain global ionospheric irregularity distributions (Pi et al., 2017). However, the resolution is not good enough to resolve ionospheric irregularity structures associated with the Es layer.

In this study, we have used GNSS data from the Japanese dense nationwide GNSS reference stations network (GEONET) sampled at a high rate (1 Hz) to obtain a high-resolution regional ROTI map to monitor the signature of the Es layer in real time. By using the monitoring system, we develop a methodology to identify the two-dimensional features of the Es layer which are *front orientation* and *propagation velocity*.

Furthermore, we propose a new method to reveal the three-dimensional Es layer structure by combining the two-dimensional features and the TEC variation of each satellite-station pair which have been developed in this study. We have applied our proposed method to reveal the structures of the Es layer in comparison to those in previous works to understand the generation and propagation mechanisms of the Es layer.

2 | DATA AND ANALYSIS METHODOLOGY

We use data from 200 GNSS stations over Japan out of about 1,300 GEONET stations. Real-time raw measurement data at a rate of 1 Hz are used. To detect small signatures of the Es layer which are often less than 1 TEC Unit (TECU, 10^{16} electrons/m^2), we used the ROTI as defined by the following equations (Pi et al., 1997):

$$ROT = \frac{TEC\,(t) - TEC\,(t - \delta t)}{\delta t} \tag{1}$$

$$ROTI = \sqrt{\langle ROT^2 \rangle - \langle ROT \rangle^2} \tag{2}$$

where *TEC(t)* is the TEC value at time *t*, δt is the time step which is 30 seconds in our analysis, and $< >$ represents the ensemble average. We derived the TEC value for each satellite using dual-frequency measurements. ROTI values with a time interval of 5 minutes were estimated by the TEC values. As the Es layer signature lasts for a very short time (often 1 minute or so), ROTI is more effective to detect such events in the 5-minute intervals rather than monitoring detrended TEC itself as the previous study (Maeda & Heki, 2014) did.

The derived ROTI values are mapped at two different altitudes, 350 km and 100 km representing the F and E regions, respectively. When the structure mapped at one of the altitudes is clear and that at the other altitude is not clear, it can be inferred that the structure-enhancing ROTI should be at the altitude with a clear structure.

From the temporal development of the ROTI structures which are determined to be from the E region, we can determine the propagation direction, and when it has a frontal structure, we can derive the front orientation as well. Once the front orientation and propagation velocity are determined, the slant TEC variation sampled at 1 Hz and used to calculate the ROTI can be inverted to the density structures across the front.

3 | RESULTS

3.1 | Detecting Es layer with ROTI

Figure 1 shows the ROTI maps observed at 05:00 UT on June 4, 2018, and projected at altitudes of 350 km and 100 km. In the ROTI map projected at an altitude of 100 km, a clear frontal structure from the west-southwest to east-northeast is seen, while the locations of enhanced ROTI values are scattered in the map projected at an altitude of 350 km.

An ionosonde station (Kokubunji, 35.71°N, 139.49°E) operated by the National Institute of Information and Communication Technology in Japan near the frontal structure detected a strong Es layer as shown in Figure 2. Therefore, it is convincing that the frontal structure shows the horizontal structure of the Es layer. It should be noted that this technique is often not applicable at night because ionospheric irregularities co-exist in the E and F regions (Saito et al., 2007).

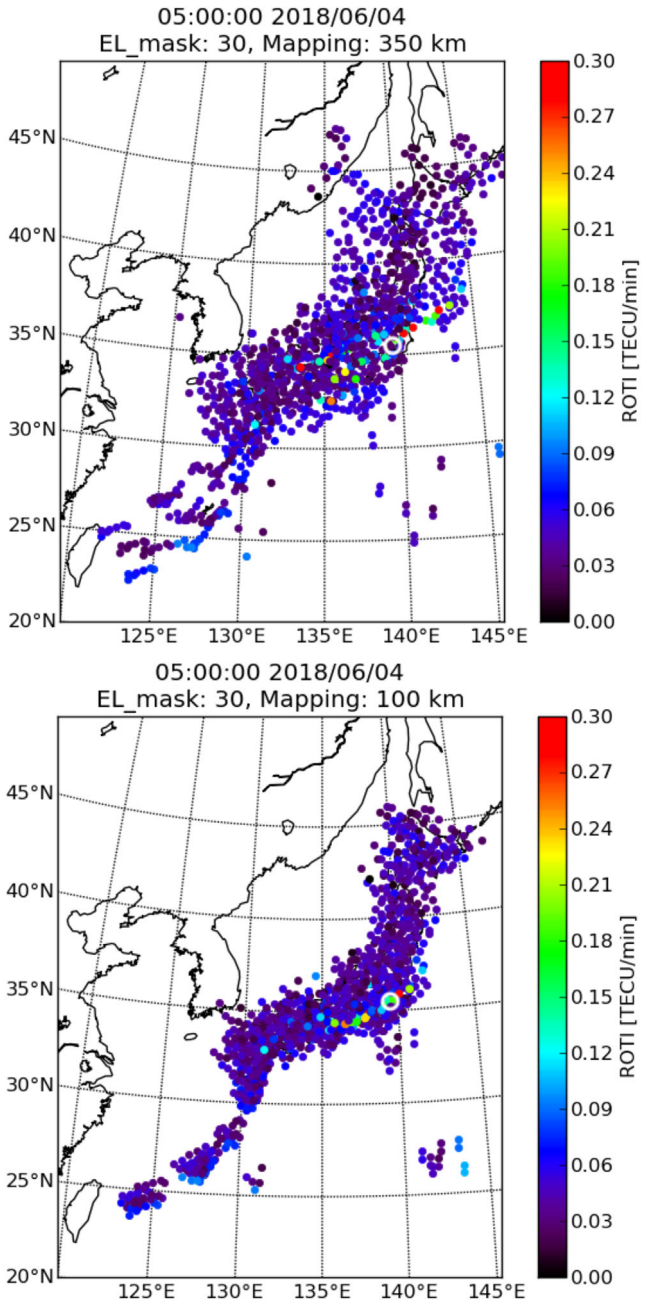

FIGURE 1 ROTI maps observed at 05:00 UT on June 4, 2018, mapped at altitudes of 350 km (top) and 100 km (bottom). White open circles indicate the location of the Kokubunji ionosonde station [Color figure can be viewed in the online issue, which is available at wileyonlinelibrary.com and www.ion.org]

Figure 3 shows the Es parameters derived from the Kokubunji ionosonde station and the ROTI values over the ionosonde site. The ionosonde parameters used are the *ftEs* and *fbEs* which are the top and blanketing frequencies of the Es layer echo, respectively, and are manually scaled by the authors. The ROTI values shown are the mean of the three largest ROTI values of which ionospheric pierce points (IPPs) are within 100 km from the ionosonde site. Variations of ftEs and ROTI values are in very good agreement and support the hypothesis that the frontal structure observed on the ROTI map surely represents the horizontal structure of the Es layer.

The differences between ftEs and fbEs are also shown in Figure 3. This difference, ftEs-fbEs, is often used to represent the inhomogeneity of the Es layer. fbEs indicates that the density of the Es layer is higher than the one corresponding to the plasma frequency anywhere in the area probed by the ionosonde, while the ftEs represents the highest density. Therefore, large ftEs-fbEs values mean large spatial variation of the Es layer density.

Some enhancements in ftEs-fbEs can be seen, although the ftEs-fbEs values were not always obtained. This is due to the low F region peak density in the local summer. The opportunity to obtain fbEs values is limited, because the fbEs value must be lower than the F region peak density in order to be detected.

We found similar ROTI enhancements on the 17th day of 28 days of observations in June 2018. Observations on two days were missing due to technical maintenance. Although close comparison with the ionosonde measurements is left for our future studies, it can be said that the ROTI map can detect a considerable number of Es layer events.

3.2 | Derivation of Es parameters from a ROTI map

To retrieve the properties of the frontal structure seen in the ROTI map, the Hough transform (Ballard, 1981; Duda & Hart, 1973) is applied. The Hough transform (hereinafter referred to as HT) is an effective way to identify a certain figure from an image. It is often used to retrieve structures automatically without manual inspection by human eyes.

In this analysis, just a simple HT is used to identify a linear structure. Figure 4 shows the ROTI map in the region in which the frontal structure is seen. This color image is first converted to a gray-scale image. Then an edge detection algorithm is applied to the gray-scale image. Finally, the HT is applied to the image which contains the information of edges in the original image.

Figure 4 also shows the line identified by HT. It can be seen that the identified line fits well to the frontal structure of the ROTI enhancement. From the result of the HT, the front direction was determined to be -20° counterclockwise from the north.

Figure 5 shows the ROTI map and the frontal structure identified by HT 15 minutes after the time of Figure 4. It can be seen that the identified frontal structure is parallel to that identified from the map 15 minutes before and displaced by 51 km to the direction normal to the frontal structure. With the frontal structures identified by the HT

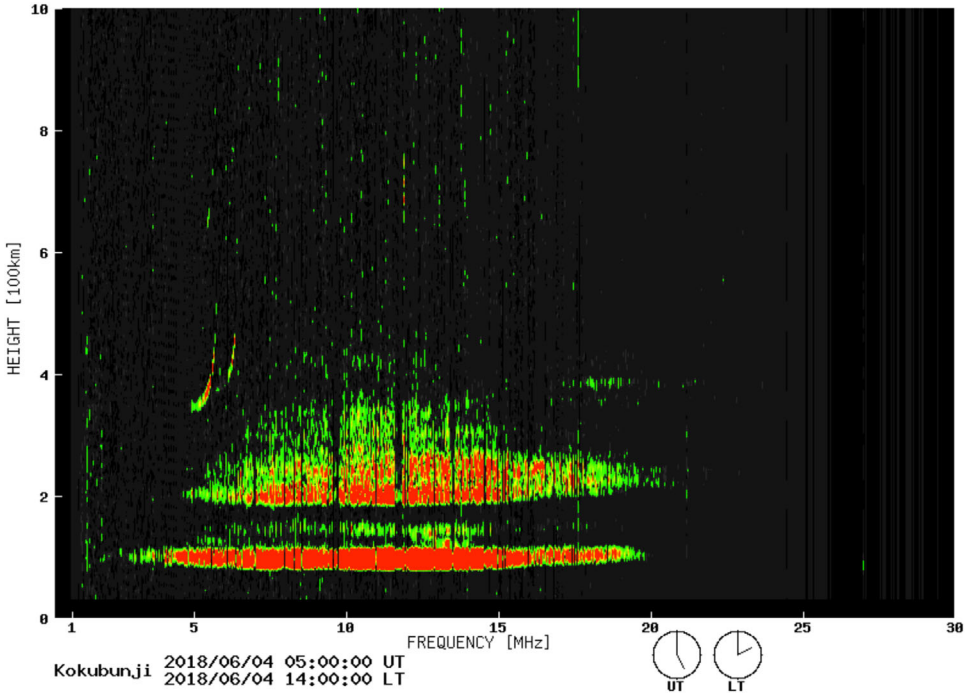

FIGURE 2 Ionogram observed at Kokubunji, Japan, at 05:00 UT on June 4, 2018 [Color figure can be viewed in the online issue, which is available at wileyonlinelibrary.com and www.ion.org]

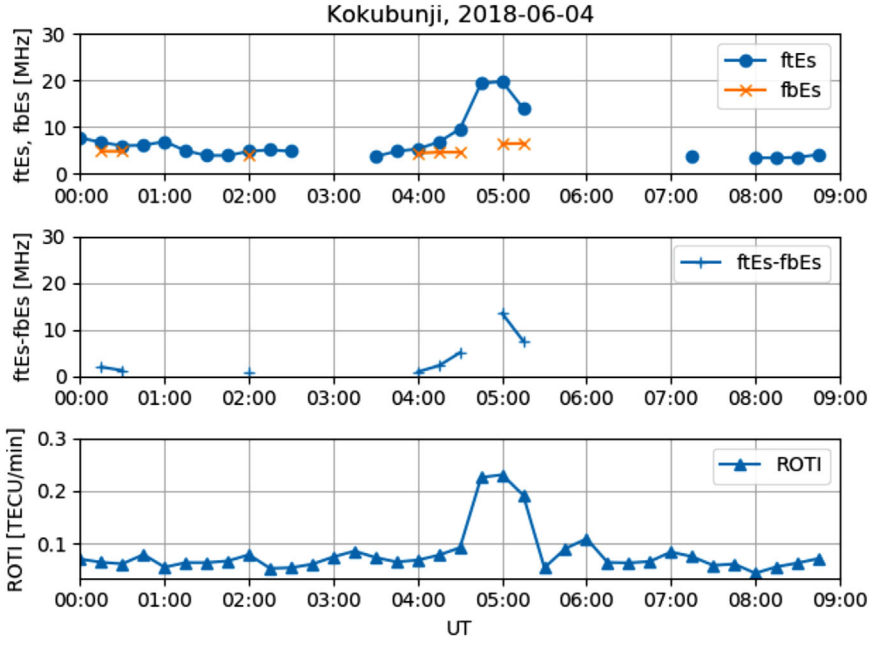

FIGURE 3 (Top): The maximum frequency reflected by the Es layer (ftEs) and the minimum frequency that can pass through the Es layer (fbEs) manually scaled from ionograms at Kokubunji; (Middle): the difference between ftEs and fbEs; and (Bottom): the maximum ROTI value over the ionosonde (Tokyo) within the radius of 100 km). All the data were collected on June 4, 2018 [Color figure can be viewed in the online issue, which is available at wileyonlinelibrary.com and www.ion.org]

of the two successive ROTI maps, the frontal structure of the Es layer can be estimated as 56 m sec^{-1}.

This velocity is consistent with the Es layer velocity reported using the TEC perturbation (Maeda & Heki, 2015). Recently, Sun et al. (2021) showed with the TEC perturbation method that the Es layer over China moved predominantly southward. To understand such differences within the northeast Asian region, more observations and comparison with numerical models such as GAIA (Andoh et al., 2020; Shinagawa et al., 2017, 2021) are necessary.

It should be noted that these processes of drawing ROTI maps, identifying Es layer structure, and deriving velocities do not require manual processing, and are thus suitable for automated Es layer detection and derivation of its structural parameters. Our technique would provide a large amount of data to contribute to

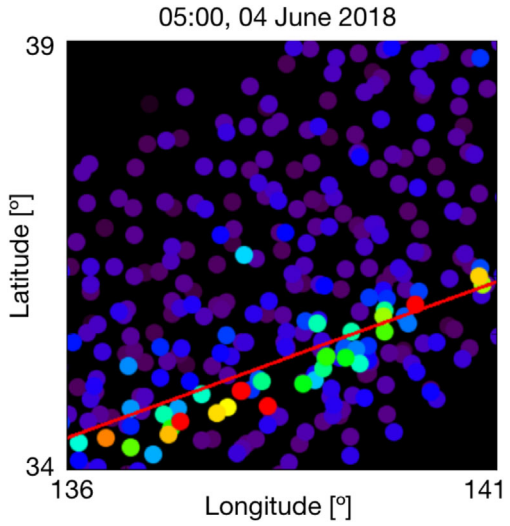

FIGURE 4 ROTI map at 05:00 UT on June 4, 2018; the red solid line shows the front identified by HT [Color figure can be viewed in the online issue, which is available at wileyonlinelibrary.com and www.ion.org]

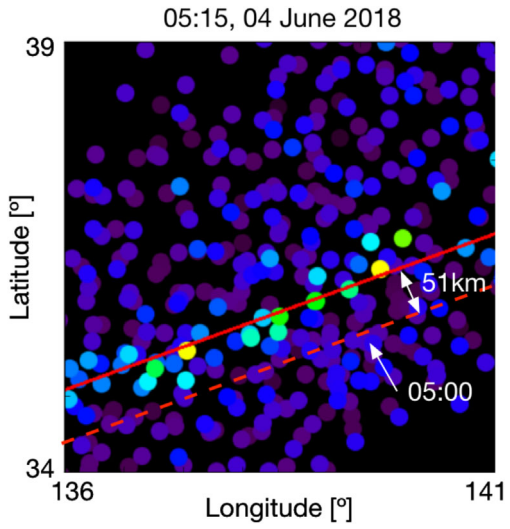

FIGURE 5 ROTI map at 05:15 UT on June 4, 2018, with a front identified by the Hough transform (red solid line); the identified front at 05:00 UT is shown by a red broken line [Color figure can be viewed in the online issue, which is available at wileyonlinelibrary.com and www.ion.org]

understanding the intra-regional variability of the Es layer characteristics.

Currently, only the ROTI map generation has been automated based on the real-time TEC perturbation mapping system (Saito et al., 2014). Integration of the automated Es layer detection and characterization to the real-time TEC perturbation/ROTI monitoring system is the nearest next step.

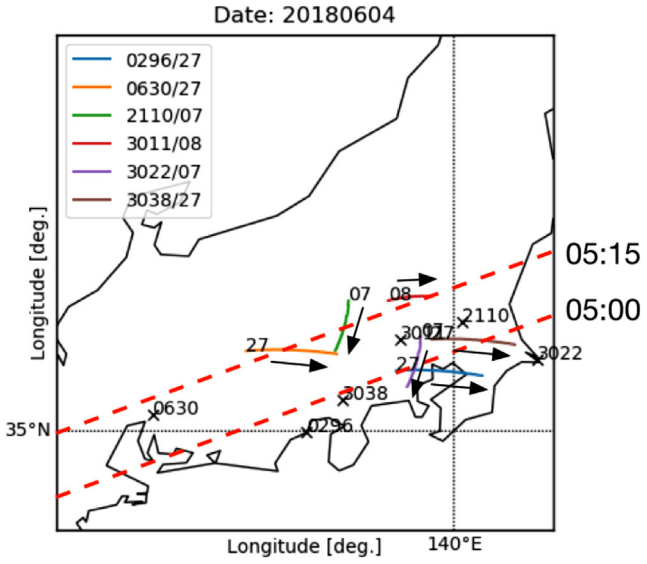

FIGURE 6 IPP traces of six receiver-satellite pairs with large ROTI values from 04:45 to 05:30 UT; the legend indicates the pairs of the receiver and satellite connected by "/"; arrows show the direction of IPP motion. The Es layer frontal structures identified by the Hough transform at 05:00 and 05:15 are also shown by red broken lines; locations of the receivers are indicated by black crosses. [Color figure can be viewed in the online issue, which is available at wileyonlinelibrary.com and www.ion.org]

3.3 | Fine structures of the Es layer

In this subsection, fine structures (i.e., the sub-structures in the Es layer front) are investigated by utilizing the TEC values sampled at a high rate (1 Hz) and the front parameters (direction and velocity) derived from the ROTI map in the previous subsection.

Figure 6 shows the IPP traces of six receiver-satellite pairs where the large ROTI values were observed. The receiver-satellite pairs corresponding to the three largest ROTI values over the ionosonde site at 05:00 and 05:15 were selected. It can be seen that four of the IPP traces evolved from the West to East and two of them evolved from the North to the South. As the Es front stretched from the west-southwest to east-northwest and moved toward the north-northwest, all IPP traces crossed the Es front from the fore-side.

Figure 7 shows the temporal variations of the slant TEC values for the six receiver-satellite pairs shown in Figure 6. In all the TEC variation, there are positive enhancements with an amplitude of about several 0.1 TECU. The ionosode shows that the maximum ftEs is greater than 20 MHz which corresponds to the electron density of about $5 \cdot 10^{12}$ m^{-3}.

If the thickness of the layer in altitude is assumed to be 1 km, the corresponding TEC is 0.5 TECU, which is comparable to the observed TEC variation. It is important

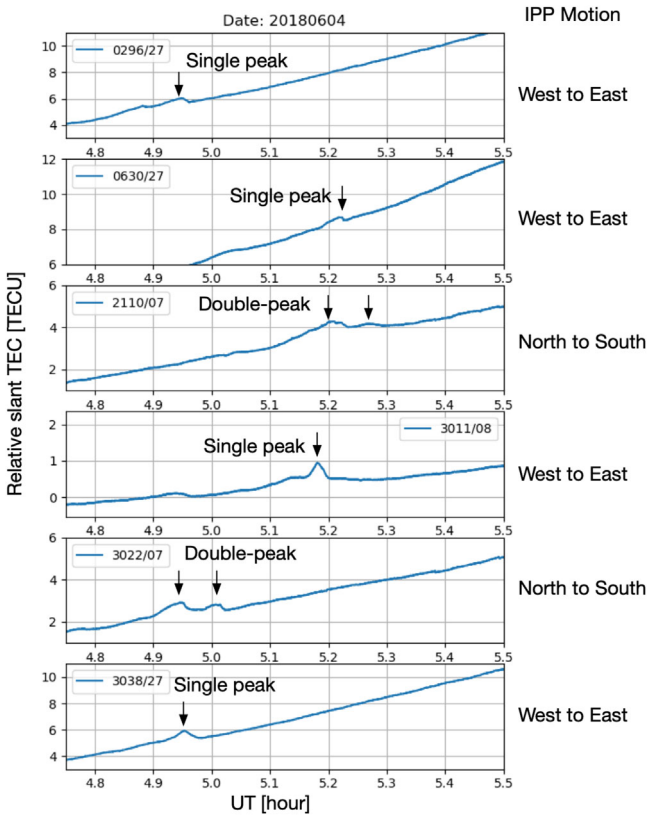

FIGURE 7 Temporal variation of the slant TEC values for the six satellite-receiver pairs shown in Figure 6. Each legend indicates the corresponding pairs of the receiver and satellite connected by "/." Vertical arrows indicate the TEC perturbation causing ROTI enhancements (for the receiver 0630 and satellite PRN27, TEC values before 4.95 hours which are smooth have been omitted). [Color figure can be viewed in the online issue, which is available at wileyonlinelibrary.com and www.ion.org]

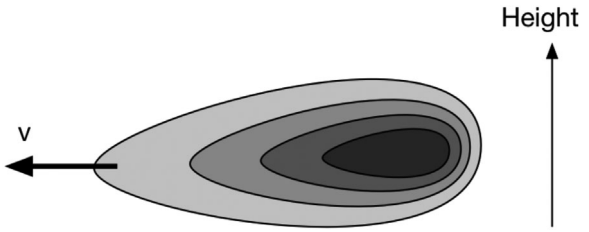

FIGURE 8 Illustration of the vertical cross-section of the Es front with a steeper density gradient on the backside than the frontside

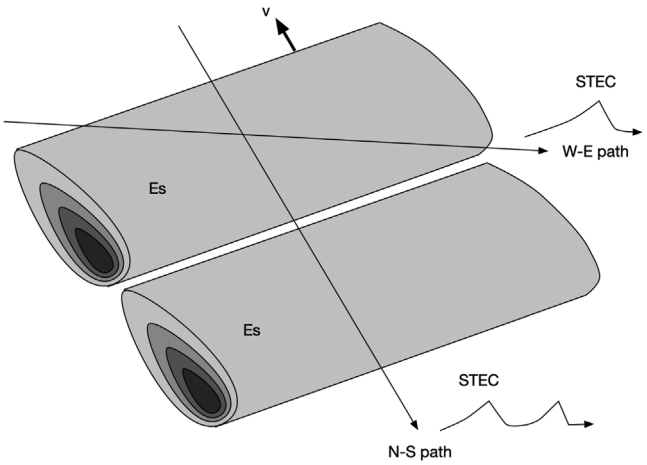

FIGURE 9 Illustration of the inferred three-dimensional shapes of the Es layer

to note that no negative perturbation is observed in the TEC, which is consistent with the hypothesis that these perturbations causing ROTI enhancements were due to the Es layer, which would add positive perturbation to the background TEC associated with the thick F region. These patterns are similar to those observed in previous works (Maeda & Heki, 2014; Muafiry et al., 2018).

The TEC enhancements occurred over 1–2 minutes. If we assume that the Es layer structure would not change in that short period of time, the temporal variation of the TEC can be interpreted as the spatial variation. The temporal variations of the TEC at the time when large ROTI values were obtained show that the TEC variations after the peak are always steeper than before the peak. As all the receiver-satellite lines-of-sight cross the Es layer from its front side, the Es layer density is asymmetrically distributed along the Es front normal direction and the density gradient is steeper at the backside than front side (as illustrated in Figure 8).

A similar structure was found in previous works by Maruyama (1991) and Maeda and Heki (2015). Maruyama (1991) suggested that the polarization electric field could be developed to form this kind of structure at night when the observation was made. As our observations were conducted in the daytime when such a polarization of the electric field would not work effectively, some other theories and/or comparison with numerical simulations of Es layer development may be necessary to understand the mechanisms that result in the inferred structure. Though further analysis is necessary to elucidate detailed structures, it is worth pointing out there that this analysis is made possible by determining the Es front parameters by the ROTI maps and HT of them.

Another interesting feature can be seen in the TEC variations seen by the receiver-satellite pairs of 2110/07 and 3022/07. For both pairs, the IPP trace crossed the Es front with a larger angle than other pairs. Both TEC variations show a double-peak structure. This indicates that the Es front might have two successive sub-fronts, each of which have a cross-section as illustrated in Figure 9.

Because of the average time interval to derive the ROTI values (which is 5 minutes), this sub-front structure cannot be resolved by the ROTI map only. By combining the

TEC values sampled at a high rate and the Es layer front direction and drift velocity derived from the ROTI maps, fine structures of the Es layer within the resolution of the ROTI maps can be inferred.

In addition to the structure across the Es front, structures along the Es front could also be resolved by compiling TEC variations from different satellite-receiver pairs. Analysis of the along-front structure of the Es layer is deferred to our future study. Furthermore, we plan to try tomographic reconstruction of the Es layer structure.

Thampi and Yamamoto (2010) used radio beacon signals from low Earth orbit (LEO) satellites to reconstruct the ionospheric density, where LEO satellites fly over the ionosphere in a short period. We have the TEC data during the Es layer events (1–2 minutes) with a good temporal resolution (1 second). By compensating for the Es layer motion by the estimated front speed and velocity, we could constitute a similar observation geometry.

4 | DISCUSSION AND SUMMARY

The ROTI map is found to be effective in detecting the Es layer structure and characterizing its frontal structure. This helps to distinguish the temporal and spatial variation of TEC along the path from the satellite to receiver. However, it should be noted that this technique is not always applicable.

As ROTI is an indicator of TEC variation, it would not be sensitive to a dense but homogeneous Es layer. For such a very flat Es layer, ROTI may be enhanced only at the edges of the Es layer. However, the Es layer would not be totally flat, and some ROTI enhancements may be expected, when the density of the Es layer is very high.

To test the detectability of the Es layer by the ROTI map, further comparison with ionosonde observations is necessary. The inhomogeneity parameter of the Es layer, ftEs-fbEs, would be a key parameter especially. Nevertheless, the ROTI map is still a useful method, because two-dimensional Es layer structures cannot be obtained continuously without GNSS network observations and the ROTI map, and the HT analysis enables automated derivation of Es layer parameters.

Another issue when using ROTI mapping in detecting the Es layer is that it is not simply applicable to the night time Es layer. In the night of local summer in the mid-latitude region, TEC perturbations in the F region often occur associated with medium-scale traveling ionospheric disturbances (MSTIDs; Saito et al., 1998). They are correlated with the appearance of the Es layer at the bottom of the F region connected by the geomagnetic field lines (Saito et al., 2007).

The amplitude of TEC perturbations associated with MSTIDs are stronger than that of the Es layer, which may mask the weak TEC perturbation associated with the Es layer. However, there are some key differences between the TEC disturbances in the F region and the Es layer.

The spatial scales appear to be larger for the MSTIDs, while it is much smaller in the Es layer (Saito et al., 2007). The IPP velocity at the F and E region heights are different by a factor of three, which would result in different apparent temporal variations of TECs for perturbations in the F region and the Es layer. This study provides a key technique to tackle these very challenging problems.

In summary, mapping ROTI is a very useful and promising technique to study the Es layer characteristics. This is realized by the very dense GNSS network with fast sampling. The technique developed in this study to detect the frontal structure of the Es layer is effective and suitable for an automatic real-time Es layer detection system. This is capable of monitoring the Es layer in a wide area and two-dimensionally.

Sub-structures of the Es layer can be investigated by combining the two-dimensional features and the TEC variation. In the studied example on June 4, 2018, the Es layer was considered to have two successive fronts with a steeper density gradient on the backside. We plan to extend our method to further investigate the three-dimensional structures of the Es layer.

Recently, long-range anomalous propagation of aeronautical VHF radio waves has been utilized to monitor the Es layer (Hosokawa et al., 2020). It can monitor a wider area where there is no GNSS network such as over the sea. On the other hand, it is not sensitive to the Es layer near the receiver of the VHF radio waves. A combination of ROTI monitoring and VHF anomalous propagation would complement each other to enable wider area Es layer monitoring.

ACKNOWLEDGMENTS

This study is partly supported by the Grant-in-aid for Scientific Research (Kakenhi) (18H04437) by Japan Society for the Promotion of Science (JSPS). This study is partly supported by the Murata Science Foundation. The ionograms used in this study are obtained and provided by the National Institute of Information and Communications Technology, Japan.

ORCID

Susumu Saito https://orcid.org/0000-0002-4645-6033
Keisuke Hosokawa https://orcid.org/0000-0001-7389-7128

REFERENCES

Andoh, S., Saito, A., Shinagawa, H., & Ejiri, M. K. (2020). First simulations of day-to-day variability of mid-latitude sporadic E layer structures. *Earth, Planets and Space*, *72*(165). https://doi.org/10.1186/s40623-020-01299-8

Ballard, D. H. (1981). Generalizing the Hough transform to detect arbitrary shapes. *Pattern Recognition*, *13*(2), 111–122. https://doi.org/10.1016/0031-3203(81)90009-1

Duda, R. O., & Hart, P. E. (1973). *Pattern classification and scene analysis*. Wiley.

Hosokawa, K., Sakai, J., Tomozawa, I., Saito, S., Tsugawa, T., Nishioka, M., & Ishii, M. (2020). A monitoring network for anomalous propagation of aeronautical VHF radio waves due to sporadic E in Japan. *Earth, Planets and Space*, *72*(88). https://doi.org/10.1186/s40623-020-01216-z

Maeda, J., & Heki, K. (2014). Two-dimensional observations of midlatitude sporadic E irregularities with a dense GPS array in Japan. *Radio Science*, *49*(1), 28–35. https://doi.org/10.1002/2013RS005295

Maeda, J., & Heki, K. (2015). Morphology and dynamics of daytime mid-latitude sporadic-E patches revealed by GPS total electron content observations in Japan. *Earth, Planets and Space*, *67*(89). https://doi.org/10.1186/s40623-015-0257-4

Maruyama, T. (1991). Observations of quasi-periodic scintillations and their possible relation to the dynamics of Es plasma blobs. *Radio Science*, *26*(3), 691–700. https://doi.org/10.1029/91RS00357

Miller, K. L., & Smith, L. G. (1975). Horizontal structure of midlatitude sporadic-E layers observed by incoherent scatter radio. *Radio Science*, *10*(3), 271–276. https://doi.org/10.1029/RS010i003p00271

Miller, K. L., & Smith, L. G. (1978). Incoherent scatter radar observations of irregular structure in mid-latitude sporadic E layers. *Journal of Geophysical Research: Space Physics*, *83*(A8), 3761–3775. https://doi.org/10.1029/JA083iA08p03761

Muafiry, I. N, Heki, K., & Maeda, J. (2018). 3D tomography of midlatitude sporadic-E in Japan from GNSS-TEC data. *Earth, Planets and Space*, *70*(45). https://doi.org/10.1186/s40623-018-0815-7

Pi, X., Mannucci, A. J., Lindqwister, U. J., & Ho, C. M. (1997). Monitoring of global ionospheric irregularities using the Worldwide GPS network. *Geophysical Research Letters*, *24*(18), 2283–2286. https://doi.org/10.1029/97GL02273

Pi, X., Iijima, B. A., & Lu, W. (2017). Effects of ionospheric scintillation on GNSS-based positioning. *NAVIGATION*, *64*(1), 3–22. https://doi.org/10.1002/navi.182

Saito, A., Fukao, S., & Miyazaki, S. (1998). High resolution mapping of TEC perturbations with the GSI GPS Network over Japan. *Geophysical Research Letters*, *25*(16), 3079–3082. https://doi.org/10.1029/98GL52361

Saito, S., Yamamoto, M., Hashiguchi, H., & Maegawa, A. (2006). Observation of three-dimensional structures of quasi-periodic echoes associated with mid-latitude sporadic-E layers by MU radar ultra-multi-channel system. *Geophysical Research Letters*, *33*(14). https://doi.org/10.1029/2005GL025526

Saito, S., Yamamoto, M., & Hashiguchi, H. (2007). Observational evidence of coupling between quasi-periodic echoes and medium scale traveling ionospheric disturbances. *Annales Geophysicae*, *25*(10), 2185–2194. https://doi.org/10.5194/angeo-25-2185-2007

Saito, S., Yoshihara, T., & Yamamoto, M. (2014). Real time ionospheric disturbance analysis and monitoring with GEONET real time data. *Proc. of the 2014 International Technical Meeting of the Institute of Navigation (ION ITM 2014)*, San Diego, CA, 720–724.

Sakai, J., Hosokawa, K., Tomizawa, I., & Saito, S. (2019). A statistical study of anomalous VHF propagation due to the sporadic-E layer in the air-navigation band. *Radio Science*, *54*(5), 426–439. https://doi.org/10.1029/2018RS006781

Shinagawa, H., Miyoshi, Y., Jin, H., & Fujiwara, H. (2017). Global distribution of neutral wind shear associated with sporadic E layers derived from GAIA. *Journal of Geophysical Research: Space Physics*, *122*(4), 4450–4465. https://doi.org/10.1002/2016JA023778

Shinagawa, H., Tao, C., Jin, H., Miyoshi, Y., & Fujiwara, H. (2021). Numerical prediction of sporadic E layer occurrence using GAIA. *Earth, Planets and Space*, *73*(28). https://doi.org/10.1186/s40623-020-01330-y

Sun, W., Zhao, X., Hu, L., Yang, S., Xie, H., Chang, S., Ning, B., Li, J., Liu, L., & Li, G. (2021). Morphological characteristics of thousand-kilometer-scale Es structures over China. *Journal of Geophysical Research: Space Physics*, *126*(2). https://doi.org/10.1029/2020JA028712

Taguchi, S. & Shibata, H. (1961). World Maps of foEs. *Journal of Radio Research Laboratory*, *8*(38–39), 355–386.

Thampi, S. V., & Yamamoto, M. (2010). First results from the ionospheric tomography experiment using beacon TEC data obtained by means of a network along a longitude of 136°E over Japan. *Earth, Planets and Space*, *62*, 359–364. https://doi.org/10.5047/eps.2009.10.003

Whitehead, J. D. (1970). Production and prediction of sporadic E. *Reviews of Geophysics*, *8*(1), 65–144. https://doi.org/10.1029/RG008i001p00065

How to cite this article: Saito S, Hosokawa K. Study of structures of the sporadic E layer by using dense GNSS network observations. *NAVIGATION*. 2021;*68*:751–758. https://doi.org/10.1002/navi.454